Waste Management 213 (2026) 115371

Contents lists available at ScienceDirect

Waste Management

journal homepage: www.elsevier.com/locate/wasman

Research Paper

From lime stabilization to CO_2 sequestration: spontaneous recarbonation in municipal sewage sludge

Felix Brück [a,*], Florian Schmutzler [a], Jan Reeh [b], Christine Fröhlich [b], Harald Platen [a], Harald Weigand [a]

[a] THM University of Applied Sciences, Centre of Competence for Sustainable Engineering and Environmental Systems (ZEuUS), Wiesenstr. 14, D-35390 Gießen, Germany
[b] THM University of Applied Sciences, Department of Mathematics, Natural Science, and Informatics (MNI), Wiesenstr. 14, D-35390 Gießen, Germany

ARTICLE INFO

Keywords:
Spontaneous recarbonation
Enhanced carbonation
Wastewater treatment plant (WWTP)
Sewage sludge
Lime
Calcium carbonate

ABSTRACT

Lime treatment is widely applied for stabilizing and conditioning municipal sewage sludge to improve handling and hygienic properties. It also offers the potential for carbon dioxide (CO_2) sequestration through lime recarbonation. Thereby, atmospheric CO_2 reacts with calcium hydroxide ($Ca(OH)_2$) to form calcium carbonate ($CaCO_3$), partly or fully offsetting process CO_2 emissions generated during lime production. However, its extent and rate are largely unexplored.

We investigated the spontaneous recarbonation of lime-treated sewage sludge using samples from two full-scale wastewater treatment plants (WWTPs). WWTP1 applies hydrated lime prior to dewatering, while WWTP2 adds quicklime after dewatering. Samples were incubated under controlled conditions for six months and analyzed using thermogravimetry–mass spectrometry (TGA–MS), X-ray diffraction (XRD), and bulk element determinations.

Progressive transformation of $Ca(OH)_2$ into $CaCO_3$ confirmed spontaneous recarbonation. Within four months, WWTP1 samples reached near-complete carbonation with rates approaching 100 % of the calcination-related process CO_2 emissions. By contrast, WWTP2 samples exhibited lower rates of recarbonation, with a maximum of ~94 %, likely due to heterogeneous lime distribution, and encapsulation of unreacted lime along with differences in lime quality.

These findings provide the first conclusive evidence for substantial spontaneous recarbonation of lime-treated sewage sludge under ambient conditions. They demonstrate that CO_2 uptake is strongly influenced by lime type, dosing strategy, and sludge composition. This establishes a robust basis for integrating lime recarbonation into carbon accounting frameworks and for evaluating the long-term carbon sink potential of lime-treated sludge, while fuel-related emissions from lime production remain outside the scope of this study.

1. Introduction

Sewage sludge is an inevitable by-product of biological wastewater treatment (Wu et al. 2020). Sewage sludge treatment generally involves an early dewatering step (Chang et al. 2023) and frequently the addition of lime (Dowling et al. 2015). The production of lime however, is associated with a considerable CO_2 footprint: CO_2 emissions arise from both fossil fuel combustion and process emissions during the process of calcination. They amount to 1.2 and 0.9 tonnes of CO_2 per tonne of quicklime (CaO) and hydrated lime ($Ca(OH)_2$), respectively, depending on the kiln technology and fuels used (EuLA, 2024a,b). This makes lime production an emitter and a hard-to-abate sector (Simoni et al. 2022). The options for decarbonising the lime industry are highlighted in the sector roadmap (EuLA, 2023a). While carbon capture and storage (CCS) technologies are currently considered the most promising mitigation pathway, their large-scale implementation involves high costs, and permission and construction of significant new national/regional infrastructure. In this context, spontaneous recarbonation and enhanced carbonation of lime in multiple applications have been extensively investigated by Grosso et al. (2020) and Campo et al. (2021). On average, 33 % of process-related CO_2 emissions can be captured through recarbonation within the first year after lime is used in the main application.

The market share of lime usage in the wastewater and sludge

* Corresponding author.
E-mail address: felix.brueck@lse.thm.de (F. Brück).

https://doi.org/10.1016/j.wasman.2026.115371
Received 19 November 2025; Received in revised form 13 January 2026; Accepted 25 January 2026
Available online 29 January 2026
0956-053X/© 2026 The Authors. Published by Elsevier Ltd. This is an open access article under the CC BY license (http://creativecommons.org/licenses/by/4.0/).

treatment sector has been estimated at 4.3 % for the reference year 2018 (Grosso et al. 2020; Campo et al. 2021). According to Grosso et al. (2020), sewage sludge liming follows either pre- or post-dewatering strategies, using hydrated lime ($Ca(OH)_2$) or quicklime (CaO). Reported addition levels reach up to 29 ± 13 % (as $Ca(OH)_2$) for pre-dewatering applications, and 21 ± 8 (centrifuge) or 33 ± 21 % (filter press) for post-dewatering scenarios (both expressed as CaO). For applications such as sewage sludge treatment, the available studies on recarbonation of lime are limited and the reported data are non-conclusive. This study aims to assess whether partial or full offsetting of process-related CO_2 emissions from lime production is achievable for this application, and to determine the specific conditions under which such offsetting is possible.

Beyond improving dewatering and sanitation, sludge liming affects organic matter mineralization. Several studies reported that lime addition can slow down microbial activity and organic matter degradation, particularly when limed sludge is stored or applied without intensive mixing (e.g. Morel and Guckert, 1983; Fang and Wong, 1999; Diniz et al., 2019). This effect may influence internal CO_2 generation during storage and thus interact with lime recarbonation processes. In addition to the named effects on dewatering, sanitation and stabilization of organic matter, sludge liming may also promote carbon sequestration through the process of recarbonation. The latter refers to the reconversion of lime into $CaCO_3$, a gas/solid reaction mediated by a water phase (Brück et al. 2018a). Recarbonation is thermodynamically favourable and takes place upon exposure of the limed sludge to CO_2. Spontaneous recarbonation relates to conditions where exposure happens without technical measures (Pape and Rueda, 2024) and at atmospheric CO_2 partial pressure (e.g. in stockpiles during storage of the limed sludge at WWTP sites or after farmland application) where the access of CO_2 is driven by diffusion.

Early studies provided qualitative evidence for the recarbonation of lime-treated sewage sludge. Mineralogical transformations from portlandite to calcium carbonate were reported using XRD and thermogravimetric methods, particularly near exposed surfaces or under storage conditions (Hsiau and Lo, 1994; Aarab et al., 2006; Husillos Rodríguez et al., 2012; Ahn and Kim, 2015). However, these studies did not provide quantitative, time-resolved data on CO_2 uptake or carbonation rates under ambient conditions thus leaving an open research question. Beyond sewage sludge, several recent studies have investigated accelerated carbonation and CO_2 fixation in alkaline sludges and recycled soils stabilized with lime- or ash-based binders (e.g. Trung et al. 2023; Thang et al., 2025). These works confirmed that lime-containing materials can effectively capture CO_2 and improve engineering properties under controlled carbonation, but they did neither address spontaneous recarbonation of municipal sewage sludge nor the operational differences between pre- and post-dewatering liming in WWTP practice.

Other than energy emissions from lime production, process emissions are reversible through lime recarbonation. In the case of limed sewage sludge, the absorbed CO_2 may either stem from the atmosphere or be provided by sludge respiration. This may partially or fully off-set the process CO_2 emissions from the calcination step in lime production. The extent of off-setting is often expressed as the carbonation rate, defined as the percentage ratio between the amount of CO_2 absorbed during recarbonation and the amount of process CO_2 emitted during calcination (EuLA, 2023b).

For applications such as sewage sludge treatment, the available studies on lime recarbonation remain scarce and largely qualitative, and reported carbonation rates are highly uncertain due to the limited and partly outdated database. In particular, quantitative, time-resolved data on spontaneous recarbonation of lime-treated sewage sludge under ambient conditions are lacking, and potential differences between pre-dewatering and post-dewatering lime application strategies have not yet been systematically assessed.

The aim of this study was therefore to determine the carbonation rate of lime-treated sludge under close to spontaneous recarbonation conditions, contributing to the broader goal of quantifying the degree to which the CO_2 process emissions during the production of lime are offset by its reconversion to calcium carbonate. Time-resolved incubation experiments were carried out in a climate chamber using real-world samples from two different wastewater treatment plants (WWTP) that had received three different liming levels, each. At WWTP1 the sewage sludge is regularly treated with $Ca(OH)_2$ prior to dewatering with a filter press. In turn, WWTP2 employs a treatment train where after dewatering with a centrifuge the stabilisation treatment happens with CaO. In time-resolved samples, the progress of organic matter mineralization and CO_2 uptake were traced employing a suite of complementary analytical methods and recarbonation was balanced against the process CO_2 emissions associated with lime production to establish the recarbonation rates for sewage sludge application.

2. Material and methods

2.1. Sampling sites and sample collection

Two German wastewater treatment plants (WWTPs) differing in their lime treatment method were selected for this study. The aim was to include representative operational strategies with respect to the timing and method of lime application. At both WWTPs, samples with three different liming levels were produced and collected, alongside blank samples (no lime) and samples of the lime used at each site. The exact lime dosing rates were not predefined by the authors but were adjusted by the plant operators under normal operating conditions to generate three distinct liming levels (low, medium, high), which included the standard application levels. Consequently, lime addition rates could not be quantified directly during sampling. The resulting lime fractions and CaO-equivalent dosages were therefore reconstructed retrospectively based on chemical analyses using a calcium mass-balance approach (Section 2.4.1). While manufacturers' technical datasheets were available for the commercial limes used at both WWTPs, detailed information on intrinsic properties governing site-specific lime behaviour (e.g., effective hydration completeness, reactivity under sludge treatment conditions, or in-situ pH buffering performance) was not available. Consequently, differences in lime behaviour are interpreted primarily based on mineralogical and thermogravimtric indicators derived from the treated sludge samples.

The following sections describe the two WWTPs in detail, including the applied lime products and their nominal specifications.

WWTP1 serves approximately a 34,000 population equivalent (PE) and receives domestic as well as industrial wastewater from a catchment area that includes small businesses and craft industries. The maximum hydraulic capacity of the plant is 614 L/s. Based on the design, the wastewater treatment process includes multiple steps: 1. Mechanical pretreatment (removal of coarse materials, sand, and grease); 2. Biological treatment with nitrification and denitrification; 3. Chemical phosphate removal using ferric chloride, and 4. Subsequent sludge conditioning and dewatering (Supplement Fig. S1). In this facility, hydrated lime is applied before dewatering. A milk of lime suspension is prepared on-site in a 1 m^3 stirred tank reactor using calcium hydroxide (PRE-CAL®50 N, SCHAEFER Kalk GmbH & Co. KG) stored in a 19-ton silo. According to manufacturer specifications, the material contains 97.4 % $Ca(OH)_2$ (calculated as total CaO) with minor impurities (MgO 0.8 %, SiO_2 0.2 %, Al_2O_3 0.08 %), a bulk density of 0.45 kg dm^{-3}, and a residual moisture of 0.5 %. The suspension is then mixed with pre-thickened raw sludge and ferric chloride and stored in an aerated buffer tank for 12–24 h preventing settling. Dewatering is carried out in batches using a chamber filter press. Three distinct liming levels (low, medium, and high) were prepared by adjusting the mixing ratio of sludge and milk of lime under otherwise normal plant operation. Dewatered sludge samples were collected from the filter cake discharge container and transferred into clamping ring drums. For the blank sample (no lime), raw sludge was taken from a pipeline nozzle before

lime addition and dewatered in the laboratory. Additionally, a representative sample of milk of lime was collected directly from the stirred reactor.

The WWTP2 serves a comparable population equivalent (approx. 35,000 PE) and primarily treats domestic wastewater. The treatment process is similar to WWPT1, but phosphate elimination is performed with a mixed iron/aluminum salt solution. Sludge dewatering happens via centrifugation (Supplement Fig. S2). In contrast to WWTP1, granular quicklime (Terradur®, ZWK Otterbein GmbH), an unslaked air lime (EN 459–1CL 80-Q) with approx. 82 % CaO + MgO is added to the centrifuge-dewatered sludge with a twin-screw mixer. The treated sludge is conveyed to a storage area via screw conveyors. Sampling was performed at the end of the conveyor line, and the sludge was directly collected into 60-liter clamping ring drums. The blank sample (no lime) was obtained by temporarily suspending the lime dosing system. Low, medium, and high liming levels were adapted by manually adjusting the dosing screw speed. The lowest setting represented the plant's standard operation, while medium and high levels were reached by increasing in the feed rate. After each change, a 20-minute stabilization period was necessary to minimize carryover effects. Representative quicklime samples were collected upstream of the mixing unit.

Due to the different liming and dewatering strategies, the samples differed in terms of compactness. The filter cakes from WWTP1 were highly consolidated. For homogenization and improved workability, the samples were manually passed through a screen sieve with a 10 mm mesh size. Other than the samples from WWTP1, the WWTP 2 material was granular and loose requiring no such pre-conditioning. Samples from both origins were immediately transported to the laboratory and were kept under refrigeration until their analytical characterization and use in the incubation experiment.

2.2. Spontaneous recarbonation test

To assess the spontaneous carbonation behaviour of lime-treated sewage sludge under laboratory simulated operational conditions, a six-month incubation test was initiated within a few days after sampling. Samples were placed in Petri dishes (diameter: 100 mm, height: 20 mm; average sample mass: 60 g) and exposed to ambient CO_2 levels in a thermostatic chamber at 20 °C with a total void volume of approximately 14 m^3. For each WWTP and liming level, 21 Petri dishes were prepared yielding three physical replications per monthly sampling event (t = 0, 1, 2, 3, 4, 5, and 6 months). At t = 0, the mass of sample was recorded by weighing. According to separate dry matter determinations the time-resolved weight gain or weight loss of the samples could be determined.

In the thermostatic chamber, a shelving unit was enclosed on all sides with foil to regulate airflow and prevent excessive odour emissions. Samples were randomly distributed across trays placed within the shelving unit to minimize bias. A schematic overview of the experimental setup, including the positioning of Petri dishes, fans, filters, sensors, and airflow paths, is provided in Fig. 1. Airflow was controlled by circulating filtered air within the shelf system. The exhaust air was passed over a gas filter (volume: 2.5 L) filled with sulfuric acid-impregnated activated carbon to minimize nuisance by typical odorants such as ammonia and recirculated to the shelf via a duct. Throughout the experiment, temperature, relative humidity, and CO_2 concentration were monitored using a multilogger system (AREXX Engineering). Throughout the six-month experiment, the temperature was stable around 20 ± 2 °C, with slightly elevated values (~1 °C) inside the sample rack due to blower operation. Relative humidity in the rack was generally higher than in the surrounding air (up to ~80 % RH), reflecting the moisture release from the sludge, and gradually decreased as more samples were removed (2 WWTP, 3 liming levels, 3 physical replications = 18 Petri dishes per month). The average CO_2 concentration inside the rack was 573 ppm, close to ambient background levels, confirming that the incubation conditions can be considered similar to ambient conditions.

To account for moisture loss by evaporation from the Petri dish surfaces, the samples were weighed weekly. Any mass loss was compensated by carefully adding appropriate amounts of distilled water. After each watering event, trays were randomly repositioned on different shelves.

2.3. Analytical

Prior to analysis, all samples underwent standardized pre-treatment steps. Samples were dried at 105 °C for a minimum of 24 h or longer as required to achieve constant dry matter conditions. The dried samples were then thoroughly ground using a Fritsch Pulverisette 6 Classic Line planetary ball mill equipped with an 80 mL tungsten carbide grinding

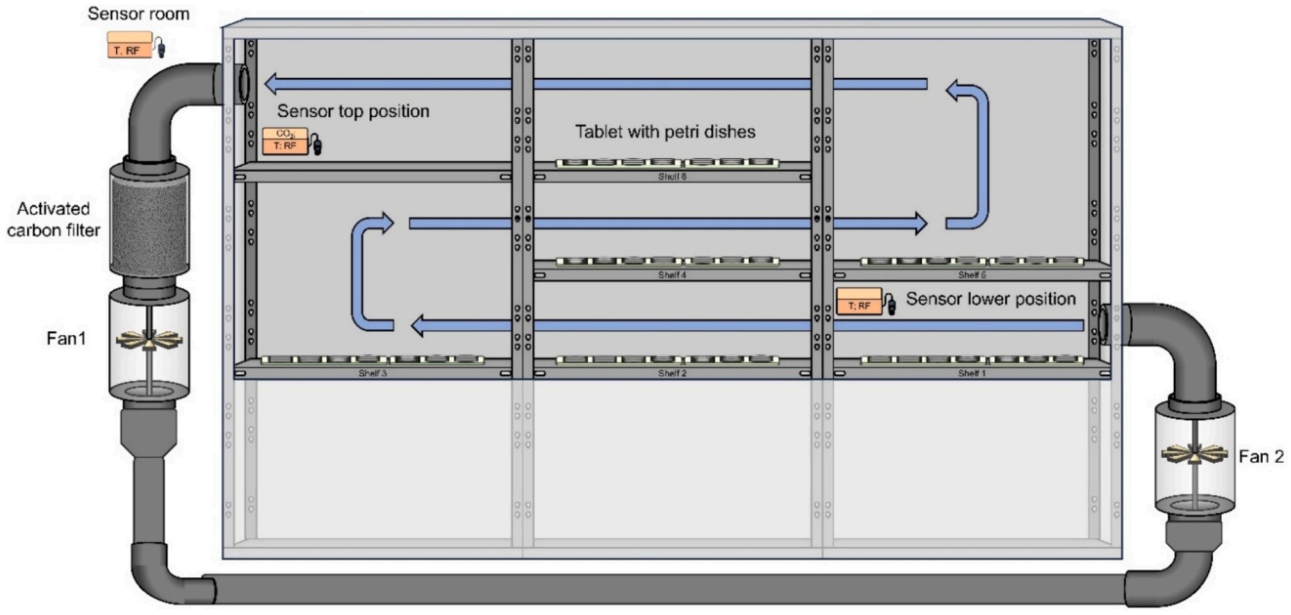


Fig. 1. Schematic experimental setup for spontaneous recarbonation test including air flow (blue arrows) and odor control. (For interpretation of the references to colour in this figure legend, the reader is referred to the web version of this article.)

bowl and 25 × 10 mm tungsten carbide balls. Grinding was conducted at 600 RPM for 460 s. Subsequently, the ground material was sieved to a particle size of less than 0.1 mm using a Retsch AS 200 control vibrating sieve machine operated at an amplitude of 1.0 mm for 5 min.

Carbon, hydrogen, nitrogen, and sulphur contents were determined in analytical triplicates by dry combustion using a Vario El cube elemental analyser equipped with a thermal conductivity detector. The inorganic carbon content was determined by subtracting the organic carbon (measured in acid-digested aliquots) from the total carbon content, providing complementary insight into the extent of carbonation and organic matter degradation. Further elements in sludge and lime samples were determined X-ray fluorescence (XRF) spectroscopy using a SpectroScout ES spectrometer with a Motex Magnum TSR-B5008-RH2 X-ray source. Measurements were conducted under helium purging with sample rotation to enhance accuracy. Thermogravimetry coupled with mass spectrometry (TGA-MS) served to assess the thermal decomposition behavior of the sludge samples. Measurements were performed using a TG 209 F1 Iris thermobalance (Netzsch), connected to a quadrupole mass spectrometer (Aëolos Quadro, Netzsch). Samples were heated from 30 °C to 900 °C at a constant rate of 10 °C·min^{-1} under a nitrogen atmosphere (flow rate: 40 mL·min^{-1}). The mass loss and its first derivative (dm/dT) were used to identify characteristic decomposition temperature ranges, particularly those associated with $Ca(OH)_2$ and $CaCO_3$. The decomposition of calcite (700–800 °C) served as a quantitative marker for lime recarbonation. Coupling with mass spectrometry enabled unequivocal attribution of the mass loss to the release of CO_2 via detection of the $m/z = 44$ ion signal.

Mineralogical characterization happened by XRD with a Bruker D2 Phaser instrument. Measurements were performed using CuKα radiation at 30 kV and 10 mA, recording diffractograms from 5° to 60° 2θ with a step size of 0.05° 2θ and 1 s acquisition time per step. Phase identification was achieved via advanced software analysis.

2.4. Calculations

2.4.1. Mass balanced change in sample composition

Quantifying the progress of recarbonation on $CaCO_3$ concentrations alone is not viable since during the incubation experiments two groups of processes may overlap: On the one hand, while a gain in sample dry matter over time can be expected from the uptake of CO_2 on the other hand a loss of dry matter may occur due to mineralization (loss of CO_2 and H_2O) and ammonia volatilization. To account for these effects, we adopted a mass balance approach in which the dry weight of each sample was recorded at every monthly sampling interval (data loss on month 2). Based on these, the concentrations of Total Carbon (TC), Total Inorganic Carbon (TIC), Total Organic Carbon (TOC), Nitrogen (N) (all in % dry matter) were converted to absolute mass $M_x(t)$ at time t according to Equation (1):

$$M_x(t) = C_x(t) \bullet DM(t) \quad (1)$$

where $C_X(t)$ is concentration relative to dry matter and DM(t) is the dry mass fraction of the sample.

To facilitate comparability and visualization, all values were normalized to a reference sample mass of 100 g dry matter at t = 0. This allowed for a consistent representation of elemental changes over time, including the comparison of measured CO_2 uptake (from TIC increase) to the theoretical CO_2 sequestration capacity based on the Steinour equation (Section 2.4.2).

2.4.2. Theoretical CO_2 uptake

The theoretical CO_2 sequestration potential ($\%ThCO_2$) of the lime-treated sewage sludge samples was estimated using a modified version of the Steinour equation (Steinour, 1947; Huntzinger et al. 2009) according to Equation (2) and considering the elemental composition and the inherent carbonate level, i.e. the $CaCO_3$ present at t = 0:

$$\%ThCO_2 = 0.785 \bullet (\%CaO - 0.56 \bullet \%CaCO_3 - 0.7 \bullet \%SO_3) + 1.091 \bullet \%MgO + 0.71 \bullet Na_2O + 0.468 \bullet (\%K_2O - 0.632 \bullet \%KCl) \quad (2)$$

While Equation (2) provides an estimate of the theoretical carbonation capacity based on the initial composition (t = 0), it does not directly quantify the actual extent of CO_2 offset achieved through lime recarbonation. In this study, the latter was quantified in terms of the carbonation rate which also includes the amount of lime reconverted to $CaCO_3$ prior to sludge liming (e.g. during storage at the WWTP).

2.4.3. Carbonation rate

In the literature, the carbonation rate is commonly defined as the percentage ratio between the amount of CO_2 reabsorbed by carbonation and the process CO_2 emissions released during lime calcination, excluding energy-related emissions (Campo et al. 2021). Process emissions result from the stoichiometric release of CO_2 from $CaCO_3$ during thermal decomposition to CaO. Under ideal conditions, carbonation rates can theoretically reach 100 %, but actual values may depend on application conditions, material reactivity, and exposure time. To assess the carbonation rate, the process CO_2 emissions associated with lime production were estimated for each liming level were determined. As it was not technically feasible to define exact liming levels during sampling at the WWTPs, the actual dosage was retrospectively calculated using a calcium mass balance according to Equation (3).

$$Y \bullet Ca_{sludge} + (1 - Y) \bullet Ca_{lime} = Ca_{mixture} \quad (3)$$

where Y is mass fraction of sewage sludge in the sludge-lime mixture, Ca_{sludge} is the calcium content in the untreated sewage sludge, Ca_{lime} is the calcium content of the lime, and $Ca_{mixture}$ is calcium content of lime-treated sludge.

Solving equation (3) for Y yields:

$$Y = \frac{\left(\frac{Ca_{mixture}}{Ca_{Sludge}} - \frac{Ca_{Lime}}{Ca_{Sludge}}\right)}{\left(1 - \frac{Ca_{Lime}}{Ca_{Sludge}}\right)} \quad (4)$$

The liming level-specific process CO_2 emissions ($CO_{2,PE}$) for the lime-treated sludge samples were calculated based on the measured CaO contents (measured by X-ray fluorescence) in lime and sludge. To express the CO_2 emissions resulting from the calcination of lime, sludge/lime ratios according to Equation (4) were used to valent CaO mass. The latter reflects the lime's precursor phase during thermal decomposition. These CaO equivalents were then multiplied by the stoichiometric mass ratio to released CO2 per mole of CaO formed during calcination:

$$CO_{2,PE} = \frac{M_{CO_2}}{M_{CaO}} \bullet \left(CaO_{lime} + CaO_{sludge}\right) \quad (5)$$

where $CO_{2,PE}$ is the process CO_2 emission related to the specific liming level [g CO_2/g dry sludge], M_{CO2} is the molar mass of CO_2 44.01 g/mol, M_{CaO} is the molar mass of CaO 56.08 g/mol, CaO_{lime} is the mass of CaO of the lime samples, and CaO_{sludge} is the mass of CaO of the sludge samples.

Finally, the carbonation rate was determined to evaluate the proportion of process-related CO_2 emissions that were reabsorbed during the spontaneous recarbonation period according to Equation (6).

$$\text{Carbonation rate}\,(\%) = \frac{CO_{2,\,measured}}{CO_{2,\,PE}} \bullet 100 \quad (6)$$

where $CO_{2,measured}$ represents the analytically determined net increase in CO_2 of the pertinent sample based on TIC determination in the monthly samples. TIC values were normalized to the initial dry mass of the limed sludge samples. This ratio reflects the extent to which process-

related CO_2 emissions from lime application were offset through spontaneous recarbonation of the lime-treated sludge under ambient conditions.

3. Results and Discussion

3.1. Initial sample characterization

Table 1 summarizes key properties of the collected sewage sludge samples at t = 0. The dry matter content ranged from 28–44 wt% for WWTP1 and from 23–33 wt% for WWTP2. At both sites, increasing lime dosage led to higher dry matter contents, a well-documented effect of lime addition (Samaras et al. 2008; Farzadkia and Bazrafshan, 2014). At WWTP2, the dry matter content at the high liming level was slightly lower than at the medium level (Table 1). This deviation does not reflect a reduced dewatering efficiency at higher lime dosage, but rather short-term operational variability of the centrifuge during sampling. The medium and low liming levels corresponded to the routine operating conditions at WWTP1 and WWTP2, respectively. Please note that the blank sample (no lime used) of WWTP1 sludge was dewatered in the laboratory and not by filter press as the other samples.

Elemental analysis confirmed that TOC dominated the TC in the blanks, while nitrogen and sulphur levels were comparable across both plants, reflecting their typical accumulation in sewage sludge. Major inorganic constituents included Fe, Si, Ca, Al, P, Mg, and K. Elevated Fe and Al contents in WWTP1 and WWTP2, respectively, reflect the site-specific phosphorus removal strategy (Figs. S1–S2). As expected, Ca concentrations increased with lime dosage, reaching up to ~ 46 wt% CaO in WWTP1, where lime is also applied to improve filter press dewaterability (Thumeyer et al. 2023).

TGA–MS analysis of the limes employed is shown and in Fig. 2 and provided phase-specific insights. The lime used at WWTP1 exhibited an initial ~ 2 wt% mass loss below 150 °C, corresponding to residual moisture evaporation, while the lime from WWTP2 showed no notable mass loss up to 300 °C. A pronounced weight loss between ~ 350–500 °C, attributed to the dehydroxylation of $Ca(OH)_2$, was more significant in WWTP1 (18.8 wt%) than in WWTP2 (10.6 wt%). These values correspond to hydrated lime contents of ~ 77.3 wt% and ~ 43.6 wt%, respectively. The MS signals at $m/z = 18$ confirmed that the observed mass loss was due to H_2O release, consistent with typical decomposition temperatures for portlandite (400–450 °C; Pan et al. 2013). Thermograms of the lime-treated sewage sludge samples are provided in the Supplementary Material (Fig. S6).

Comparison of CaO-equivalents derived from $Ca(OH)_2$ and $CaCO_3$ with total CaO by XRF (see Table S1) revealed notable discrepancies. For WWTP1, the difference was minor (~7.7 wt%), indicating that most Ca occurred as portlandite or calcite. In WWTP2, however, the gap was much larger (~39.5 wt%), suggesting a significant fraction of Ca remained as unhydrated CaO or was bound in phases such as silicates, aluminates, or sulfates which decompose outside considered TGA temperature windows. The higher MgO content of the WWTP2 lime (3.0 wt %) likely contributed to the gap, since MgO-rich quicklimes are known to hydrate more slowly and at lower peak temperatures. This may have reduced the detected amount of portlandite (Potgieter et al. 2003; Leontakianakos et al. 2017).

In the blank samples, total weight loss of 40–60 wt% was dominated by organic matter decomposition, accompanied by characteristic signals for H_2O (m/z 18), CO_2 (m/z 44), and light hydrocarbons (m/z 26). Overlapping mineral and organic decomposition is illustrated in 3D TGA–MS plots of the raw sludge (Fig. S3). Despite this overlap, the distinct decomposition ranges of portlandite (~400–450 °C) and calcite (~650–800 °C) remained discernible, consistent with previous studies (Husillos Rodriguez et al. 2012; Magdziarz and Werle, 2014).

Complementary XRD analysis confirmed the above-named findings (Fig. S7). WWTP1 lime exhibited sharp portlandite reflections (2θ ≈ 18.0°, 34.1°, 47.1°) with minor calcite, consistent with hydrated lime partially recarbonated during storage (Galván-Ruiz et al. 2009). The blank sample from WWTP1 showed an amorphous hump (15–30° 2θ) with a weak quartz reflection (~26.6° 2θ), while limed samples revealed progressively stronger portlandite and calcite peaks with increasing liming level (Fig. S8 and S9). Quartz was consistently present, whereas Al- or Fe-bearing phases remained below the XRD detection limit.

In WWTP2, portlandite and calcite were also identified, though portlandite peaks were weaker and broader and calcite reflections more pronounced than in WWTP1and agreed with the TGA–MS results. Increasing lime dosage enhanced the intensity of these reflections, yet overall peak heights remained lower than at WWTP1. Traces of sulfate-bearing phases were additionally detected, consistent with the quicklime properties.

Taken together, these results demonstrate that hydrated lime was the dominant constituent at both WWTPs, but with clear differences in reactivity and pre-carbonation state. The WWTP1 lime was largely

Table 1
Selected characteristics of the sewage sludge samples from wastewater treatment plants (WWTP) 1 and 2.

	WWTP1				WWTP2			
Liming level	None	Low	Medium[*c]	High	None	Low[*c]	Medium	High
Dry matter (wt%)	27.96[*a]	28.46	31.32	43.93	23.22	27.83	36.88	32.76
pH L/S 40/1 (–)	6.1	11.2	11.6	12.5	7.7	9.1	10.5	12.0
Lime fraction, Y[*b] (–)	–	0.28	0.32	0.64	–	0.13	0.23	0.28
Major components (wt%)								
TC	33.29	21.50	20.72	10.33	27.06	24.50	21.98	20.28
TOC	32.19	21.60	19.31	7.98	26.50	23.75	21.89	18.86
TIC CHNS	1.10	0.20	1.41	2.35	0.48	1.03	0.62	1.43
S	0.77	0.41	0.36	0.15	0.53	0.52	0.45	0.40
N	4.93	3.03	2.86	1.31	4.10	3.44	3.08	2.78
CaO	2.71	23.35	26.73	49.96	3.29	12.45	19.57	23.03
MgO	1.47	0.97	0.95	0.69	0.75	0.87	1.22	1.31
SiO_2	10.91	5.97	5.14	2.53	13.95	12.39	12.24	11.71
Fe_2O_3	5.77	8.29	7.01	3.35	4.61	3.81	3.45	3.22
Al_2O_3 XRF	3.83	2.32	1.84	1.32	9.65	7.53	7.29	6.80
K_2O	0.91	0.40	0.37	0.28	0.66	0.64	0.68	0.67
Na_2O	<0.01	0.67	0.73	1.28	<0.01	0.18	0.34	0.48
S	0.77	0.50	0.45	0.25	0.67	0.64	0.62	0.58
Cl	0.02	1.24	0.95	0.70	0.02	0.04	0.05	0.07

[*a] Raw sludge from pre-thickener dewatered with a laboratory centrifuge,
[*b] CaO-equivalent lime dosage (kg CaO eq. per kg dry sludge according to Eq. (3).
[*c] standard liming levels of WWTP 1 and 2.

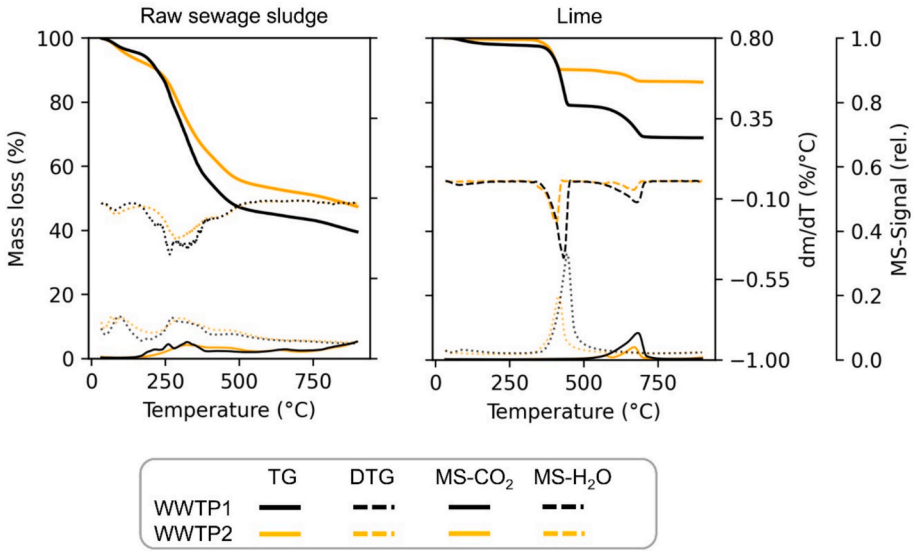


Fig. 2. TG, DTG, and MS signals (CO_2, H_2O) of raw sewage sludges (left) and lime samples (right) from WWTP1 and WWTP2.

hydrated and readily available for carbonation, while the lime used at WWTP2 exhibited a lower degree of hydration, as indicated by the reduced portlandite content observed by TGA-MS and XRD. This suggests incomplete conversion of CaO to $Ca(OH)_2$ after application, which

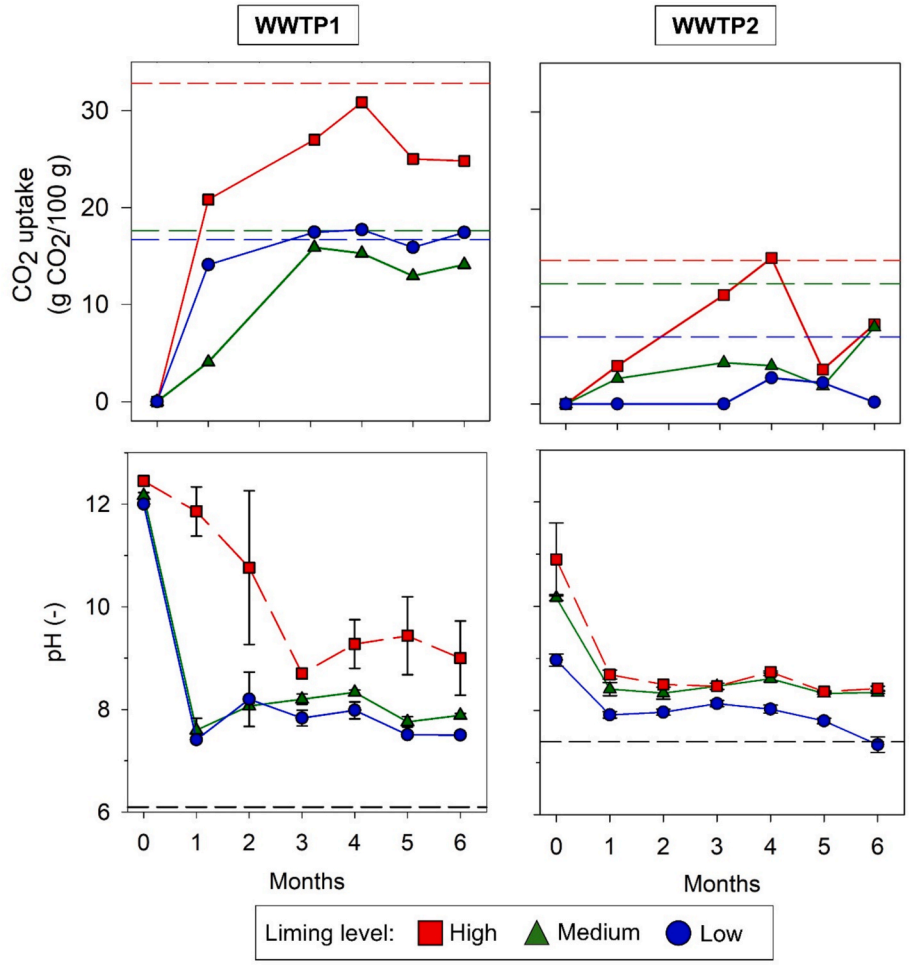


Fig. 3. Temporal evolution of CO_2 uptake (top row) and leachate pH (bottom row) during six months of spontaneous recarbonation of lime-treated sewage sludge. Results are shown for three liming levels (high, medium, low). CO_2 uptake values were derived from TIC measurements and normalized an initial dry mass of 100 g per sample. Dashed lines in the upper graphs represent the theoretical uptake potential (Equation (2). Dashed lines in the lower graphs show the pH of the blank samples.

may be related to lower lime reactivity or less favourable hydration conditions rather than the presence of 'non-hydrated' lime as a compositional characteristic. Information on the intrinsic reactivity or burning conditions of the commercial limes used at the two WWTPs was not available; therefore, interpretations regarding lime reactivity are based on indirect mineralogical and thermal indicators.

3.2. Time-dependent compositional changes in limed sewage sludge

The time-dependent concentrations of total nitrogen, sulfur, TC, TOC, TIC, and carbonate-bound carbon ($CaCO_3$-C) are shown in Figs. S4 and S5 (Supplement). Over the six-month incubation, nitrogen levels decreased markedly during the first three months (consistent with ammonia volatilization under alkaline conditions) and then stabilized. Sulfur showed no systematic trend, with fluctuations likely due to sample heterogeneity. In the following we focus on the pH, TIC, TOC, and mass balance (Figs. 3 and 4) as relevant recarbonation indicators. Since the concentration data are affected by changes in dry matter, they were converted into absolute mass using Equation (1) and referenced to an initial sample weight of 100 g.

Low liming level: At both WWTPs, the pH dropped rapidly to ~ 8 within the first month and remained near-neutral thereafter. For WWTP1, this coincided with a sharp rise in TIC and CO_2 uptake, reaching the theoretical uptake potential by month 3. In contrast, TIC for WWTP2 remained nearly unchanged until month 3 and ultimately achieved only ~ 50 % of %ThCO_2. This delayed TIC increase may be related to the comparatively low initial pH at the low liming level, which likely allowed continued microbial activity during the first months of incubation.

Consistently, TOC decreased steadily for both samples, while continuous mass loss indicates that organic matter degradation outweighed the weight gain by carbonation. In the case of WWTP2, the pronounced TOC decline provides additional evidence that microbial processes dominated the early incubation phase and may have masked or counteracted early-stage CO_2 uptake by carbonation.

Medium liming level: For both WWTPs, the pH declined quickly and stabilized at ~ 8. In WWTP1, TIC increased until month 4 and then declined gradually, resulting in a net CO_2 loss during the later incubation periods. In WWTP2, TIC increases occurred only after month 4–5, suggesting delayed spontaneous recarbonation, likely hindered by inhomogeneous lime distribution or reduced CO_2 accessibility. TOC decreased similarly in low and medium LL for WWTP1. For WWTP2, however, TOC loss was smaller in the medium LL variant, which is explained by the nearly doubled lime content (see Table 1). That may have provided a stronger alkaline buffer that reduced microbial activity and slowed organic matter degradation (see section 1).

High liming level: High lime content sustained elevated pH values for a longer period. In WWTP1, the pH decreased gradually from ~ 12 to ~ 9, reflecting the strong buffer capacity. TIC rose steadily, reaching ~ 32 g CO_2/100 g by month 4, indicating substantial CO_2 uptake. The maximum TIC was reached slightly later than the minimum pH value. TOC remained stable during the first month and decreased only gradually thereafter, while net mass gain confirmed that in this case spontaneous recarbonation outweighed organic matter degradation. In WWTP2, the pH decreased more gradually compared to WWTP1 and stabilized at ~ 8.2. TIC increased until month 4 approaching %ThCO_2 but declined thereafter so that by the end of the incubation only ~ 85 % remained. TOC degradation was minor, while mass loss after month 4

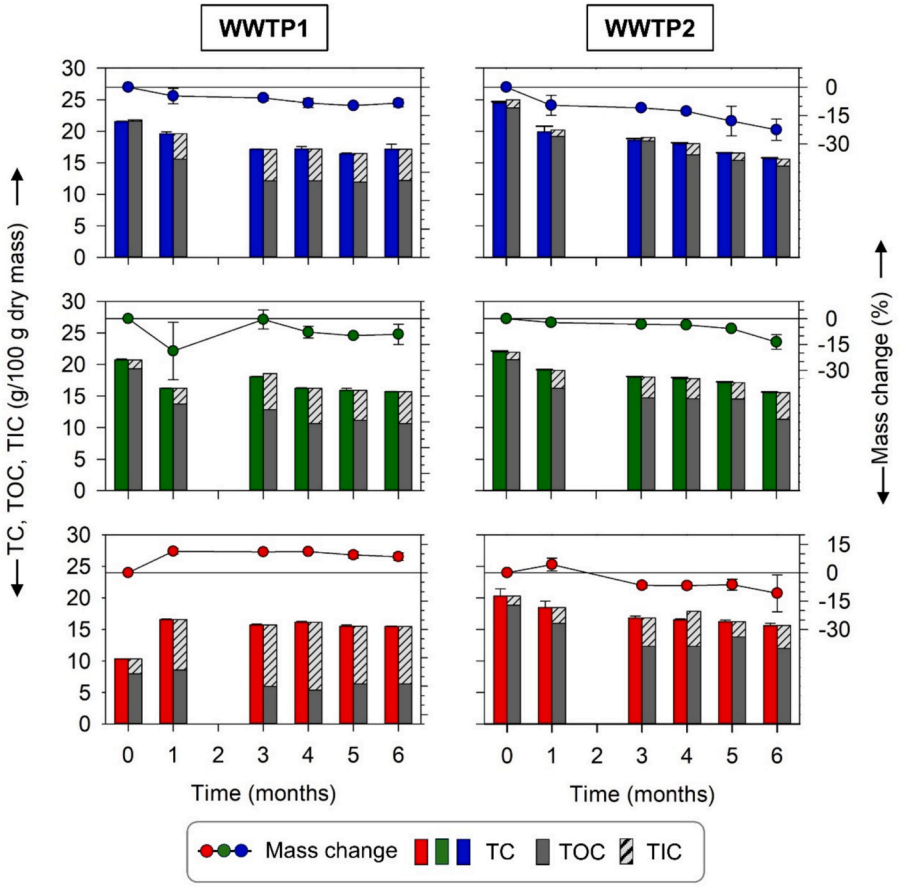


Fig. 4. Evolution of carbon fractions and mass change during spontaneous recarbonation of lime-treated sewage sludge at different liming levels (normalized to 100 g initial sample dry mass). Rows from top to bottom: High (red), medium (green), low (blue) liming levels. (For interpretation of the references to colour in this figure legend, the reader is referred to the web version of this article.)

suggests that organic matter mineralization partly offset earlier DM-gains caused by CO_2 uptake. Across all liming levels, pH values showed pronounced temporal variability, which complicates a direct temporal alignment of pH minima and TIC maxima.

For both WWTPs, several samples exhibited a decline in TIC after an initial increase. This effect was most pronounced in medium liming levels of WWTP1 and in medium and low LL of WWTP2, but was also detectable in the high liming levels samples. TIC reduction was typically accompanied by a drop in pH into the range of 7–8.

Under such near-neutral conditions, $CaCO_3$ is thermodynamically stable in pure water, but dissolution may occur if pore water becomes undersaturated with respect to calcite, for instance due to local acidification from organic matter degradation or the presence of complexing agents. Laboratory and field studies confirm that calcite solubility rises below pH ~ 8.3 and dissolution becomes significant below pH ~ 7.5 (Berner, 1978; Plummer et al. 1978; Morse et al. 2007). While pH-driven dissolution provides a plausible explanation, sample heterogeneity and microscale variation in CO_2 fluxes likely also contributed.

Moisture conditions are known to strongly influence carbonation kinetics, and alternating drying and rewetting cycles may affect CO_2 diffusion and reaction rates (Brück et al., 2018b). In this study, periodic water addition was applied as a pragmatic compromise to prevent rapid desiccation of the thin sludge layers under laboratory conditions and to enable the investigation of spontaneous recarbonation over extended time periods. While such moisture fluctuations may introduce variability, they also reflect realistic storage conditions and were applied consistently across all samples, thereby minimizing systematic bias between treatments.

Furthermore, sieving of the WWTP1 filter cake samples inevitably increased the exposed surface area compared to the untreated, highly

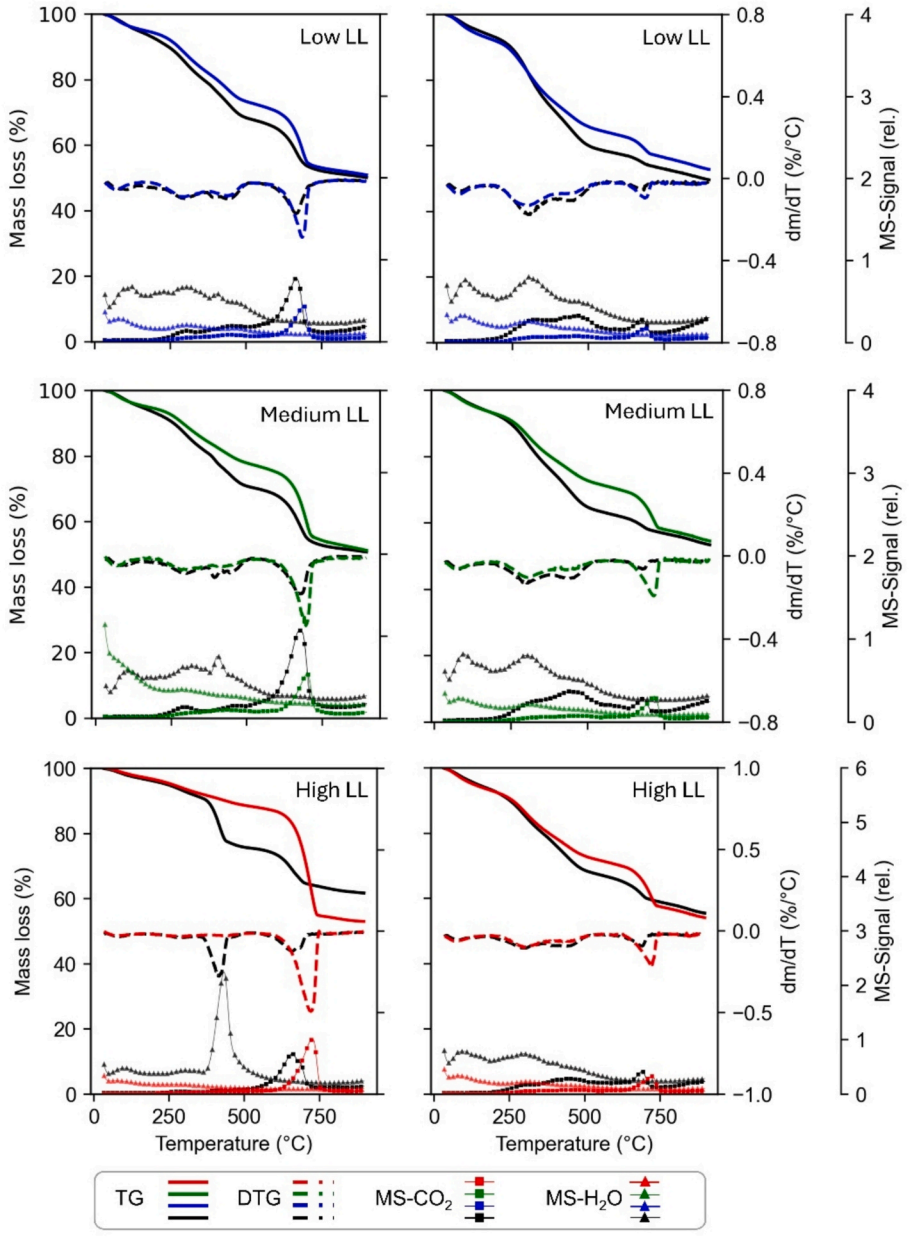


Fig. 5. Thermogravimetric, derivative thermogravimetric, and mass spectrometric (MS) signals of lime-treated sewage sludge samples from WWTP1 (left) and WWTP2 (right) at the beginning of spontaneous recarbonation (t = 0, black lines/symbols) and after 6 months of incubation (blue, green and red lines/symbols) with different liming levels (LL) namely low, medium, and high, respectively). (For interpretation of the references to colour in this figure legend, the reader is referred to the web version of this article.)

consolidated material. This may have locally enhanced CO_2 accessibility and carbonation kinetics at particle interfaces. However, given the overall dense structure of the dewatered sludge matrix and the comparatively thin incubation layers used in this study, this effect is expected to be limited and does not affect the comparative interpretation between liming levels within the same WWTP.

3.3. Changes in thermal decomposition pattern

To complement the evidence for recarbonation progress, TGA–MS was performed on selected samples from the beginning (t = 0) and the end of the six-month incubation (Fig. 5).

The data confirm that the thermal decomposition of sewage sludge typically occurs in three main stages: (i) moisture release below ~ 180 °C, (ii) organic matter degradation between ~ 200–550 °C, and (iii) decomposition of carbonates and other mineral phases above ~ 600 °C (Magdziarz and Werle, 2014). In lime-treated sludge, the second stage partly overlaps with the dehydroxylation of portlandite ($Ca(OH)_2$; ~400–450 °C) and is followed by the decarbonation of calcite or other carbonates (~650–800 °C).

The above reactions were distinguished by their characteristic gas evolution, namely H_2O ($m/z = 18$) from $Ca(OH)_2$ dehydroxylation and CO_2 ($m/z = 44$) from carbonate decomposition. The TGA–MS profiles revealed consistent shifts between initial and incubated samples, in line with the TIC-based CO_2 uptake data (Fig. 3). Most notably, the H_2O-related MS signal in the 350–500 °C range decreased strongly over the incubation period, indicating progressive consumption of portlandite. Simultaneously,

CO_2 release in the 600–800 °C window increased, reflecting enhanced carbonate content. These changes were evident across all liming levels but most pronounced in the high liming levels samples of WWTP1, consistent with their higher initial $Ca(OH)_2$ content and greater absolute carbonation capacity.

The thermogravimetry results were corroborated by XRD analysis of the high liming level samples after six months. In both WWTP1 and WWTP2, portlandite peaks that were clearly visible at t = 0 had almost completely disappeared by t = 6 months, while calcite reflections intensified (Fig. S8 and S9). This transformation from portlandite to calcite confirms the near complete carbonation of the dosed lime under the experimental conditions.

Taken together, the strong agreement between TGA–MS, XRD, and TIC data provides robust evidence that lime in sewage sludge undergoes substantial to near-complete spontaneous recarbonation within a few months of exposure. These findings further substantiate the pH and mass balance trends discussed above and underline that the extent of recarbonation scales with the initial lime content and its mineralogical state.

3.4. Carbonation rate

The carbonation rate is defined as the percentage ratio of the CO_2 absorbed during recarbonation of lime to the process CO_2 emissions from the calcination step of lime production. This metric reflects the overall degree of CO_2 uptake, irrespective of when it occurs, and thus differs from the theoretical uptake potential, which is based the state of the samples at the beginning of the experiment and subtracts any previous carbonation (e.g., during storage of lime prior to use).

To account for both, the process-related emissions and the actual uptake, the carbonation rate was calculated from the lime-specific process CO_2 footprint and the dry matter–adjusted TIC values measured throughout the six-month spontaneous recarbonation tests. Fig. 6 summarizes the maximum carbonation rate achieved for each liming level, alongside the corresponding mean and range of replicate values. For comparison, the initial degree of pre-carbonation at t = 0 (WWTP1: 14.6 %; WWTP2: 2.8 %) is also shown as grey bars.

At WWTP1, all liming levels reached or slightly exceeded full recarbonation within four months, with maximum rates of ~ 88–101 %. Values above 100 % may reflect contributions from additional carbonatable constituents (e.g., MgO, K_2O, Na_2O) or sample heterogeneity.

Overall, these findings underline the good accessibility of lime when added prior to dewatering and confirm the consistent trends observed in TIC, TGA–MS, and XRD analyses.

In contrast, none of the WWTP2 samples achieved full recarbonation. The high liming level variant reached a maximum of ~ 94 %, whereas medium and low liming level samples remained substantially lower (51 % and 27 %, respectively). Notably, these two variants also exhibited the strongest pH decline during incubation (Fig. 3), with final values close to or below the calcite saturation threshold. In addition, the comparatively lower portlandite contents observed for WWTP2 imply a reduced pH buffering capacity, as $Ca(OH)_2$ effectively buffers pH during carbonation. A faster pH decline may therefore have limited sustained carbonation, particularly once near-neutral conditions were reached. This supports the interpretation that partial carbonate dissolution or locally acidic microenvironments contributed to the lower net recarbonation rates. In addition, the post-dewatering quicklime addition at WWTP2 likely caused a heterogeneous lime distribution, preserving unreacted CaO cores in lime nodules and limiting CO_2 access.

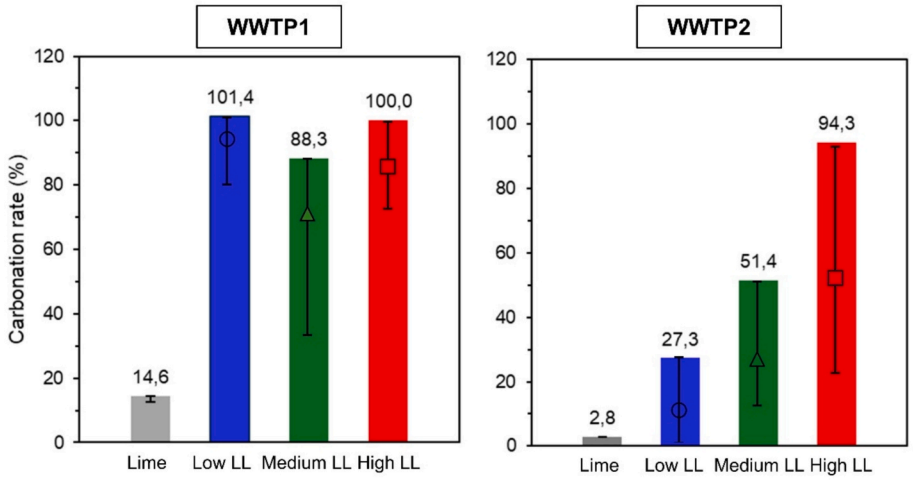


Fig. 6. Carbonation rate of lime-treated sewage sludge samples from WWTP1 (left) and WWTP2 (right) during six months of spontaneous recarbonation. Bars indicate the maximum values observed for each liming level (low = blue, medium = green, high = red), while adjacent symbols represent the mean values with range across the incubation period. Grey bars show the initial carbonation rate at t = 0, reflecting the degree of lime recarbonation prior to the experiment. (For interpretation of the references to colour in this figure legend, the reader is referred to the web version of this article.)

Taken together, these results confirm that spontaneous recarbonation of lime in sewage sludge proceeds rapidly under laboratory simulated operational conditions, with most CO_2 uptake occurring within the first three to four months. However, the extent of recarbonation is strongly influenced by the mode and timing of lime application. Whereas the configuration at WWTP1 enabled nearly complete transformation of $Ca(OH)_2$ to $CaCO_3$, the lower rates at WWTP2 highlight the sensitivity of carbonation efficiency to sludge treatment practice. The findings demonstrate that reactive lime added for sludge conditioning is progressively converted into stable carbonates, thereby acting as a relevant sink for atmospheric CO_2.

Previous assessments of lime recarbonation, such as the work Grosso et al. (2020), classified wastewater and sewage sludge treatment as a potentially relevant but still inconclusive recarbonation pathway due to lack of conclusive experimental evidence. By providing quantitative, time-resolved data from real full-scale wastewater treatment systems, the present study reduces key uncertainties identified in earlier assessments and contributes to establishing a more robust basis for the future integration of sewage sludge recarbonation into carbon accounting frameworks.

4. Conclusion

This study addressed the lack of quantitative, time-resolved data on spontaneous recarbonation of lime-treated sewage sludge by investigating samples from two full-scale wastewater treatment plants (WWTPs) applying distinct liming strategies. WWTP1 applied hydrated lime prior to dewatering via filter press, whereas WWTP2 used quicklime after centrifuge dewatering.

The results provide clear evidence that lime-treated sewage sludge can reabsorb substantial amounts of atmospheric CO_2 under ambient conditions. At WWTP1, most samples achieved recarbonation rates close to their theoretical potential within three to four months, thereby compensating most of the calcination-related (process) CO_2 emissions associated with lime production. In contrast, WWTP2 samples reached lower recarbonation rates (maximum ~ 85 % at high lime dosage), likely due to heterogeneous lime distribution, reduced gas–solid contact, and incomplete hydration.

Differences between the two WWTPs further highlight that the effective hydration, buffering capacity, and carbonation behavior of lime depend not only on nominal product specifications but also on site-specific application and mixing conditions, which could not be fully characterized based on available lime datasheets.

Overall, the findings demonstrates that spontaneous recarbonation is strongly governed by lime type, dosing strategy, and the mixing efficiency. From an operational perspective, the results indicate that allowing sufficient post-treatment storage time for lime-treated sewage sludge can enable substantial spontaneous recarbonation under ambient conditions. In systems, where limed sludge is temporarily stored prior to further processing, disposal, or land application, spontaneous recarbonation may therefore occur naturally and contribute to reducing calcination-related CO_2 emissions without additional process steps.

However, this study was also subject to limitations. Incubation experiments were conducted under controlled laboratory conditions that may not fully represent variable full-scale storage environments, and only two WWTPs and a limited range of liming strategies were investigated. Uncertainties further arise from sample heterogeneity and analytical constraints of TIC determination, TGA–MS, and XRD. Future research should therefore include field-scale monitoring of limed sludge stockpiles under diverse climatic and storage conditions to further refine the integration of lime recarbonation into carbon accounting frameworks.

CRediT authorship contribution statement

Felix Brück: Writing – original draft, Project administration, Methodology, Investigation. **Florian Schmutzler:** Methodology, Investigation. **Jan Reeh:** Visualization, Software, Formal analysis. **Christine Fröhlich:** Supervision, Resources, Methodology, Investigation. **Harald Platen:** Writing – review & editing, Supervision, Investigation, Conceptualization. **Harald Weigand:** Writing – review & editing, Writing – original draft, Supervision, Resources, Project administration, Funding acquisition, Conceptualization.

Declaration of competing interest

The authors declare the following financial interests/personal relationships which may be considered as potential competing interests: All authors reports financial support was provided by European Lime Association. If there are other authors, they declare that they have no known competing financial interests or personal relationships that could have appeared to influence the work reported in this paper.

Acknowledgement

This work was funded by the European Lime Association (EuLA). We thank the EuLA experts for fruitful technical discussions to shape the project, select the test sites and develop the laboratory operational conditions for the measurements.

Appendix A. Supplementary material

Supplementary data to this article can be found online at https://doi.org/10.1016/j.wasman.2026.115371.

Data availability

Data will be made available on request.

References

Aarab, T., Smeyers, M., Remy, M., Godden, B., Delhaye, J.P., 2006. The storage of sewage sludge: influence of liming on the evolution of copper chemical fractions. Waste Manag. 26, 1024–1032. https://doi.org/10.1016/j.wasman.2005.10.007.

Ahn, C.M., Kim, C.G., 2015. Assessments of CO_2 biomineralization and its kinetics using indigenous microorganisms derived from landfill cover soil. Desalin. Water Treat. 54, 3632–3638. https://doi.org/10.1080/19443994.2014.922280.

Berner, R.A., 1978. Equilibrium, kinetics, and the precipitation of magnesian calcite from seawater; discussion. Am. J. Sci. 278 (10), 1475–1477. https://doi.org/10.2475/ajs.278.10.1475.

Brück, F., Schnabel, K., Mansfeldt, T., Weigand, H., 2018a. Accelerated carbonation of waste incinerator bottom ash in a rotating drum batch reactor. J. Environ. Chem. Eng. 6, 5259–5268. https://doi.org/10.1016/j.jece.2018.08.024.

Brück, F., Fröhlich, C., Mansfeldt, T., Weigand, H., 2018b. A fast and simple method to monitor carbonation of MSWI bottom ash under static and dynamic conditions. Waste Manag. 78, 588–594. https://doi.org/10.1016/j.wasman.2018.06.042.

Campo, F.P., Tua, C., Biganzoli, L., Pantini, S., Grosso, M., 2021. Natural and enhanced carbonation of lime in its different applications: a review. Environ. Technol. Rev. 10, 224–237. https://doi.org/10.1080/21622515.2021.1982023.

Chang, H., Zhao, Y., Xu, A., Damgaard, A., Christensen, T.H., 2023. Mini-review of inventory data for the dewatering and drying of sewage sludge. Waste Manag. Res. 41, 1081–1088. https://doi.org/10.1177/0734242X221139170.

Diniz, I., Matos, A., Matos, M., Borges, A., Wilken, A., 2019. Degradation rate of limed sewage sludge in an agricultural soil. Environ. Eng. Manag. J. 18, 1049–1055. https://doi.org/10.30638/eemj.2019.101.

Dowling, A., O'Dwyer, J., Adley, C.C., 2015. Lime in the limelight. J. Clean. Prod. 92, 13–22. https://doi.org/10.1016/j.jclepro.2014.12.047.

EuLA – European Lime Association, 2023a. A pathway to negative CO_2 emissions by 2050. 40 pp.

EuLA – European Lime Association, 2024a. EPD-Hydrated Lime. EPD-IES-0013450:001 (S-P-13450) - Hydrated Lime - Sector EPD (https://www.environdec.com/library/epd13450).

EuLA – European Lime Association, 2023b. Lime as a natural carbon sink. Examples of mineral carbonation in lime applications. Brussels, 31.

Fang, M., Wong, J.W.C., 1999. Effects of lime amendment on availability of heavy metals and maturation in sewage sludge composting. Environ. Pollut. 106, 83–89. https://doi.org/10.1016/S0269-7491(99)00056-1.

Farzadkia, M., Bazrafshan, E., 2014. Lime stabilization of waste activated sludge. Health Scope 3 (3). https://doi.org/10.17795/jhealthscope-16035.

Galván-Ruiz, M., Hernández, J., Baños, L., Noriega-Montes, J., Rodríguez-García, M.E., 2009. Characterization of calcium carbonate, calcium oxide, and calcium hydroxide

as starting point to the improvement of lime for their use in construction. J. Mater. Civ. Eng. 21 (11), 694–698. https://doi.org/10.1061/(ASCE)0899-1561(2009)21:11(694).

EuLA - European Lime Association, 2024b. EPD-Quicklime, EPD-IES-0013480:001 (S-P-13480) - Quicklime - Sector EPD (https://www.environdec.com/library/epd13480).

Grosso M., Biganzoli L., Campo F. P., Pantini S., Tua C. 2020. Literature review on the assessment of the carbonation potential of lime in different markets and beyond. Report prepared by Assessment on Waste and Resources (AWARE) Research Group at Politecnico di Milano (PoliMI), for the European Lime Association (EuLA). 333 pp.

Hsiau, P.-C., Lo, S.-L., 1994. Characteristics of four alkaline biosolids produced from sewage sludge. Resour. Conserv. Recycl. 21, 185–197. https://doi.org/10.1016/S0921-3449(97)00035-9.

Huntzinger, D.N., Gierke, J.S., Kawatra, S.K., Eisele, T.C., Sutter, L.L., 2009. Carbon dioxide sequestration in cement kiln dust through mineral carbonation. Environ. Sci. Technol. 43 (6), 1986–1992. https://doi.org/10.1021/es802910z.

Husillos Rodríguez, N., Granados, R.J., Blanco-Varela, M.T., Cortina, J.L., Martínez-Ramírez, S., Marsal, M., Guillem, M., Puig, J., Fos, C., Larrotcha, E., Flores, J., 2012. Evaluation of a lime-mediated sewage sludge stabilisation process. Product characterisation and technological validation for its use in the cement industry. Waste Manage. 32, 550–560. https://doi.org/10.1016/j.wasman.2011.10.021.

Leontakianakos, G., Baziotis, I., Ekonomou, G., Delagrammatikas, G., Galbenis, C.T., Tsimas, S., 2017. A case study of different limestones during quick lime and slaked-lime production. Bull. Geol. Soc. Greece 43 (5), 2485. https://doi.org/10.12681/bgsg.11654.

Magdziarz, A., Werle, S., 2014. Analysis of the combustion and pyrolysis of dried sewage sludge by TGA and MS. Waste Manag. 34 (1), 174–179. https://doi.org/10.1016/j.wasman.2013.10.033.

Morel, J.L., Guckert, A., 1983: Influence of limed sludge on soil organic matter and soil physical properties. In: Catroux G, L'Hermite P, Suess E (eds): The Influence of Sewage Sludge Application on Physical and Biological Properties of Soils. Springer, Dordrecht.

Morse, J.W., Arvidson, R.S., Lüttge, A., 2007. Calcium carbonate formation and dissolution. Chem. Rev. 107 (2), 342–381. https://doi.org/10.1021/cr050358j.

Pan, S.Y., Chiang, P.C., Chen, Y.H., Tan, C.S., Chang, E.E., 2013. Ex situ CO_2 capture by carbonation of steelmaking slag coupled with metalworking wastewater in a rotating packed bed. Environ. Sci. Technol. 47 (7), 3308–3315. https://doi.org/10.1021/es304975y.

Pape, C., Rueda, O., 2024. Carbon accounting of recarbonation in lime products – Main considerations for compliance and voluntary carbon markets. South Pole Carbon Asset Management Ltd., Zurich, 39 pp.

Plummer, L.N., Wigley, T.M.L., Parkhurst, D.L., 1978. The kinetics of calcite dissolution in CO_2-water systems at 5–60 °C and 0.0–1.0 atm CO_2. Am. J. Sci. 278 (2), 179–216. https://doi.org/10.2475/ajs.278.2.179.

Potgieter, J.H., Potgieter, S.S., de Waal, D., 2003. An empirical study of factors influencing lime slaking. Part II: lime constituents and water composition. Water SA 29 (2), 157–160. https://doi.org/10.4314/wsa.v29i2.4850.

Samaras, P., Papadimitriou, C.A., Haritou, I., Zouboulis, A.I., 2008. Investigation of sewage sludge stabilization potential by the addition of fly ash and lime. Chemical Oxidation for Aqueous-Phase Contaminants 154 (1–3), 1052–1059. https://doi.org/10.1016/j.jhazmat.2007.11.012.

Simoni, M., Wilkes, M.D., Brown, S., Provis, J.L., Kinoshita, H., Hanein, T., 2022. Decarbonising the lime industry: state-of-the-art. Renew. Sustain. Energy Rev. 168. https://doi.org/10.1016/j.rser.2022.112765.

Steinour, H.H., 1947. The system CaO–SiO_2–H_2O and the hydration of the calcium silicates. Chem. Rev. 40 (3), 391–460. https://doi.org/10.1021/cr60127a003.

Thang, B.A., Hayano, K., Yamuchi, H., Anh, T.T.P., 2025. Impact of accelerated carbonation on geotechnical properties of recycled soil from construction sludge stabilized with paper sludge ash-based stabilizer and blast furnace cement. Results Eng. 28, 108044. https://doi.org/10.1016/j.rineng.2025.108044.

Trung, N.D., Sakaguchi, A., Hayano, K., Yamauchi, H., 2023. Effects of several factors in accelerated carbonation on neutralization and carbon dioxide capture of alkaline sludges treated with paper sludge ash-based stabilizer. Case Stud. Constr. Mater. 19, e02215. https://doi.org/10.1016/j.cscm.2023.e02215.

Thumeyer, L., Fröhlich, P., Dohrn, M., Wallus, S., Neuroth, M., Bertau, M., 2023. Seasonal variations in the composition of sewage sludge in the observation of a sewage treatment plant. Chem. Ing. Tech. 95, 1988–1998. https://doi.org/10.1002/cite.202300090.

Wu, B., Dai, X., Chai, X., 2020. Critical review on dewatering of sewage sludge: influential mechanism, conditioning technologies and implications to sludge reutilizations. Water Res. 180, 115912. https://doi.org/10.1016/j.watres.2020.115912.